CHAPTER 3

MECHANISMS OF MATERIAL REMOVAL IN THE CMP PROCESS

The Chemical Mechanical Polishing (CMP) process is now widely employed in the manufacture of Ultra-Large-Scale Integrated (ULSI) circuits. Yet, the effects of various process parameters on the material removal rate (MRR) and the resulting surface topography are not well understood. In this chapter, accordingly, several polishing models are reviewed with emphasis on the mechanical aspects of CMP. Experiments are conducted to verify the mechanical polishing models and to identify the dominant mechanism of material removal under typical CMP conditions. The effects of such important process parameters as the hardness of material being polished, pad stiffness and the abrasive size on MRR, Preston constant, wear coefficient, within-wafer nonuniformity and surface roughness are investigated. Process optimization schemes for enhancing MRR and Preston constant and for meeting the process specifications are also proposed.

3.1 Introduction

The main objectives of CMP are to smooth surface topography of dielectric deposits to enable multilevel metallization, or to remove excess coating material to produce inlaid metal damascene structures and shallow isolation trenches. Although CMP's ability to achieve global planarity and produce scratch-free surfaces has been proven, the mechanisms of material removal are still not clearly understood. The various models developed so far, although significant, only addressed partial aspects of the process (Brown et al., 1981; Cook, 1990; Yu, 1993; Runnels and Eyman, 1994; Liu et al., 1996; Sundararajan et al., 1999).

Although CMP is now extensively used for fabricating integrated circuits, the polishing process itself finished optical lens for several centuries. Sir Isaac Newton (1695) observed that scratch size decreases as abrasive size is decreased. By using very fine grain abrasives, he noted, it is possible to continually fret and wear away the glass and produce a polished surface on which the scratches become too small to be visible. Along the line of this hypothesis, Lord Rayleigh found that the polishing process produces highly reflective, structureless facets in a discontinuous fashion (Rayleigh, 1901). Further polishing does not improve the quality of the facets but extends their boundary. He suggested that the difference between polishing and grinding can occur by changing the character of the backing without altering the grit size. In polishing, a smaller force is applied on the abrasive by a soft, yielding backing and therefore removes material on a much finer scale, perhaps on the molecular level. Later research showed that polishing and grinding are not fundamentally different (Aghan and Samuels, 1970). Very fine-scale scratches were found on the polished metal surfaces by phase-contrast illumination, even though they look perfectly smooth under ordinary light. Experiments also showed that brittle fracture occurs on ceramic surfaces under certain circumstances (Komanduri et al., 1997).

Another line of research suggested that polishing is the result of surface melting (Beilby, 1921; Bowden and Hughes, 1937). Proposed by Beilby and developed by Bowden and Hughes, this hypothesis states that the asperities on the surface might reach melting temperature during contact rubbing. The melt would smear from the high spots over the depressions and thus produce a smooth surface. It was shown that the material removal rate strongly correlates with the melting point of the material being polished, not with its hardness. However, later research showed that the correlation does not hold for materials with high melting temperature, and that the material removal rate depends on the relative hardness at the temperature of rubbing conditions, which implies some sort of abrasion mechanism (Rabinowicz, 1968; Samuels, 1971).

In addition to the abrasion and melting mechanisms, adhesion was also considered as a means of material removal in polishing (Rabinowicz, 1968). He proposed that when two sliding surfaces are in contact elastically under a light load, the adhesion force tends not to remove material as substantial fragments. Because excessive energy is required to remove

these high surface-to-volume ratio fragments, the surface material will be stripped off from the high spots on a molecular scale. The rate of material removal does depend, however, on the strength of the chemical bonds between molecules, which is measured in terms of the latent heat of evaporation. However, no direct evidence has been presented to prove that adhesion indeed plays an important role in polishing.

Recently, much attention has been paid to the effects of chemicals in the polishing slurry. Chemicals can effectively improve the polishing rate and reduce scratching (Cook, 1990; Komanduri et al., 1997; Luo et al. 1998). Some researchers have suggested that chemical action, enhanced by mechanical stress and temperature, is the dominant factor in polishing because material on molecular-scale cannot be achieved by mechanical abrasion alone.

Nevertheless, the material removal rate (MRR) for various coatings is empirically found to proportionally increase with the product of applied pressure and relative velocity, which may be expressed as (Preston, 1921):

$$\frac{dh}{dt} = k_p p v_R \tag{3.1}$$

where h is the thickness of the layer removed, t the polishing time, p the nominal pressure, v_R the relative velocity, and k_p is a constant known as the Preston constant. It may be noted that Eq. (3.1) can be used on both local and global scales. When it is employed to estimate the average removal rate across the wafer surface, the thickness removed should be much larger than the variation in surface roughness. In tribology, the wear equation is another way to represent the volume worn in sliding or abrasive wear situations (Holm, 1946; Archard, 1953):

$$V = k_w \frac{LS}{H} \tag{3.2}$$

where V is the volume removed, L the load on the sample, S the relative sliding distance, H the hardness of the worn material concerned, and k_w is the wear coefficient. It may be noted

that the wear equation is concerned only with the total worn volume, regardless whether the surface is worn uniformly. The wear coefficient, to a first approximation, can be used to categorize the wear processes, i.e., the wear coefficient will be approximately the same for various materials if the wear mechanism is the same.

In this chapter, the mechanisms of polishing are investigated and several polishing theories are examined experimentally. Models relevant to wafer usual polishing practice, which includes a compliant pad and a common abrasive and the range of pressure and velocity at common operations, are established. Different aspects of the process, such as the material hardness, abrasive size, pad stiffness and its porous structure, are addressed and correlated with friction coefficient, material removal rate, Preston constant, and wear coefficient. The variation of material removal rate across the wafer is also addressed. Finally, a process optimization scheme based on the models and experimental results is proposed.

3.2 Experimental

All test specimens were in the form of 1 μm thick coatings on 100-mm diameter p-type (111) silicon wafers. The coatings were Al, Cu, SiO_2 (PECVD), SiO_2 (TEOS), and Si_3N_4. A 20 nm TiN as an adhesion layer was sputter-coated for the Al and Cu coatings. The SiO_2 thin films were deposited on the wafers using silane or by TEOS (tetraethyloxysilane) by a PECVD process. The Si_3N_4 film was deposited by a LPCVD process. Table 3.1 lists the density, melting temperature, modulus of elasticity, and Poisson's ratio of the coatings. The hardness of the films was measured by Knoop microindentation. The results are also shown in Table 3.1.

The polishing experiments were conducted on a rotary-type polisher. Table 3.2 lists the experimental conditions. A wafer was held in the recess of the wafer carrier and pressed against a polishing pad at a constant normal pressure of 48 kPa for each experiment. The wafer carrier and the pad were rotated at 75 rpm to maintain a constant relative velocity of 0.7 m/s across the wafer. These conditions ensure that polishing was conducted in the contact

Table 3.2: Experimental conditions.

Experimental Parameters	Present Work	Typical CMP Conditions
Diameter of Wafer (mm)	100	200
Normal Load (N)	391	1,297 - 1,565
Normal Pressure (kPa)	48	41 - 48
Rotational Speed (rpm)	75	25 - 40
Linear Velocity (m/s)	0.70	0.5 - 0.8
Duration (min)	1 - 4	2 - 4
Sliding Distance (m)	42 - 168	60 - 192
Slurry Flow Rate (ml/min)	150	100 - 200
Abrasive	α-Al_2O_3	SiO_2, Al_2O_3
Abrasive Size (nm)	50, 300, 1000	150 - 300
pH	7	3 - 4 for metals 9 - 10 for ceramics

mode. This was verified by monitoring the friction forces in two orthogonal directions on the wafer with load sensors. Table 3.2 also lists the operating conditions of typical CMP practice for comparison with those of the present work. In addition to the 300 nm α-Al_2O_3 abrasives used in common CMP practice, two other sizes of Al_2O_3 particles were employed to study the size effects. A neutral slurry was used to focus only on the mechanical aspects of the polishing process.

Two types of commercial polyurethane pads, shown in Figs. 3.1 and 3.2, were used. The Buehler CHEMOMET pad is a lighter, softer 1 mm thick pad composed of irregular, interconnected pores of an average diameter of 15 μm. Pore size increased three to four times and the matrix density decreased in the bottom third of the pad. The Rodel IC-1400 pad comprises two stacks. The top is a stiff 1.3 mm thick stack with spherical, isolated pores of 40 μm in diameter. In addition, concentric grooves, 500 μm wide, 750 μm deep, with a 1.5 mm pitch are molded onto the surface to enhance wafer-scale slurry dispensing. The bottom stack comprises a lighter 1.3 mm thick foam with interconnected pores twice as large as those of the top pad. The room temperature elastic moduli of the top and bottom pads were about 500 MPa and 60 MPa, respectively.

The average Material Removal Rate (MRR) for each coating was determined by weighing the wafer before and after polishing. For the SiO_2 coatings, the thickness was measured by ellipsometry at 49 fixed sites across the wafer to determine the local removal rate and the Within-Wafer Nonuniformity (WIWNU). The polished surfaces were examined in a Scanning Electron Microscope (SEM) and by an Atomic Force Microscope (AFM) to characterize surface roughness and surface scratches.

3.3 Results

3.3.1 Friction Coefficient. Figures 3.3 and 3.4 show the friction coefficient plotted against polishing time for different coating materials on both the Buehler and Rodel pads with 300 nm Al_2O_3 abrasive slurry. The polishing time was varied so that the coatings were not polished through. The friction coefficient, except at the beginning, remains constant

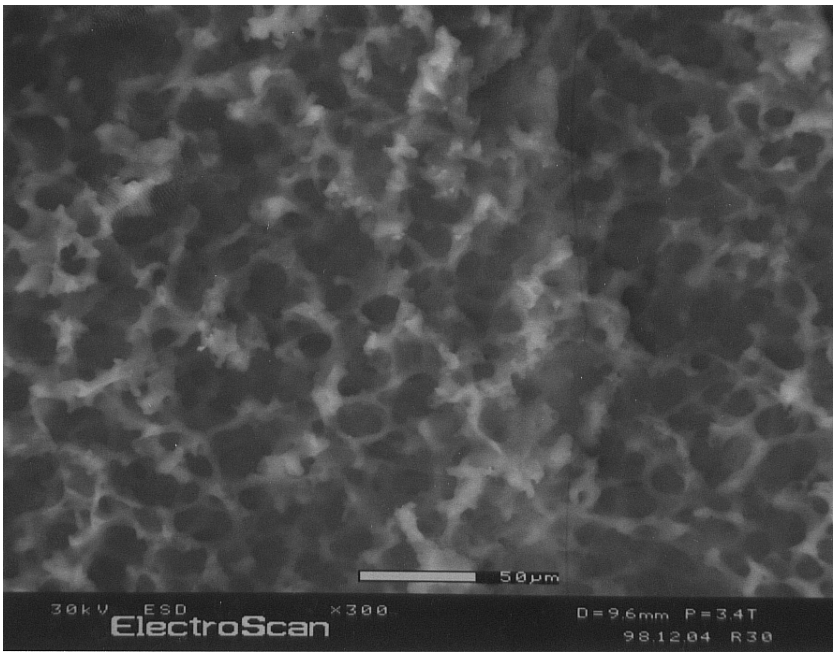

(a)

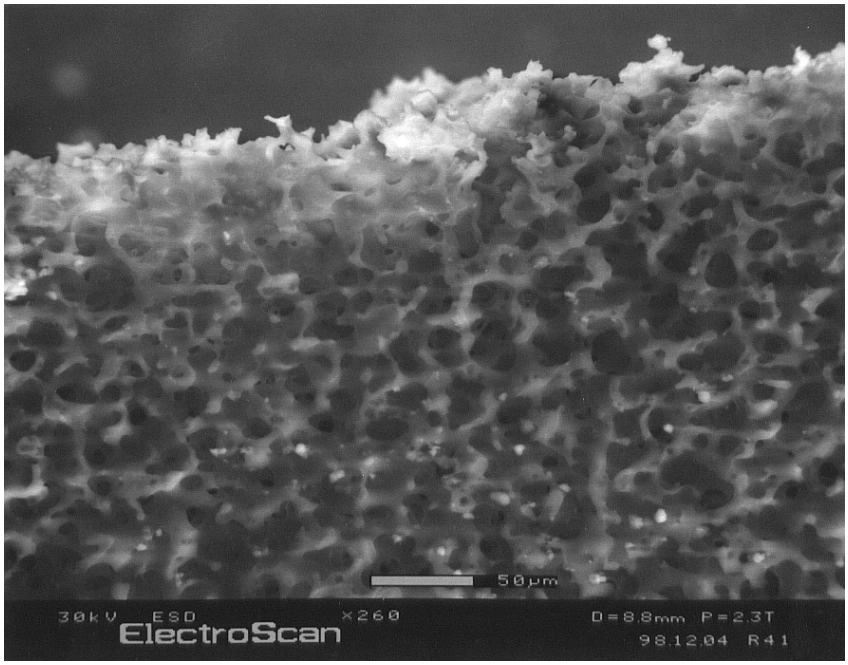

(b)

Figure 3.1 SEM micrographs of Buehler CHEMOMET pad: (a) top surface and (b) cross-section near the top surface.

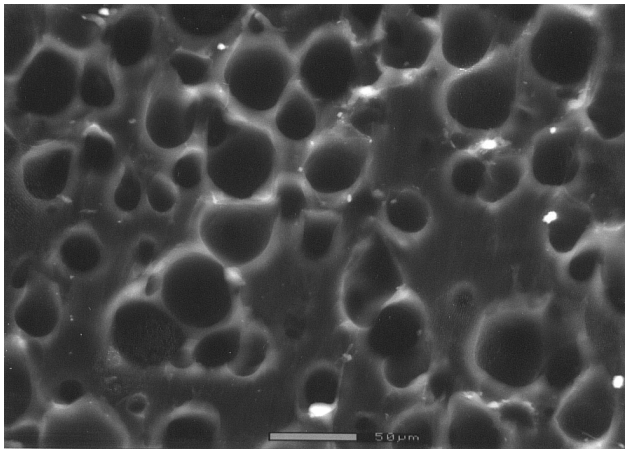

(a)

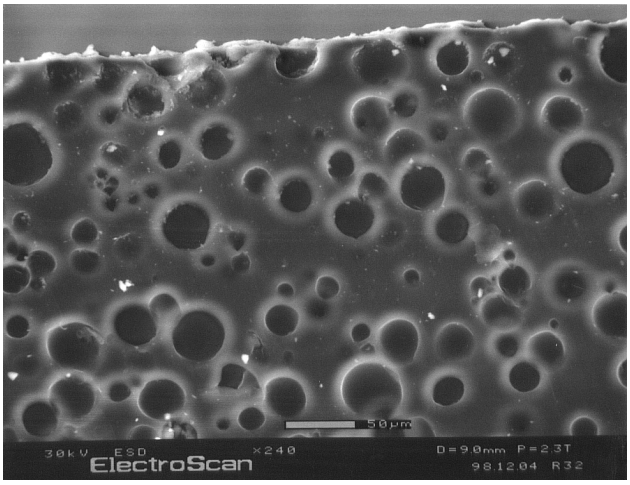

(b)

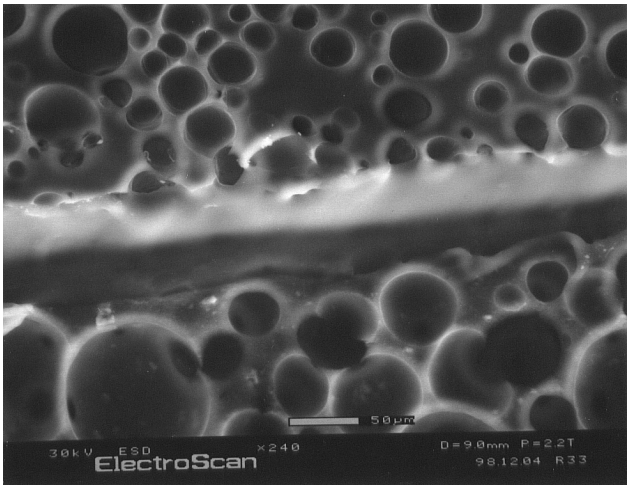

(c)

Figure 3.2 SEM micrographs of Rodel IC-1400 pad: (a) top surface, (b) cross-section of the top stack, and (c) cross-section at the interface between the top and the bottom stacks.

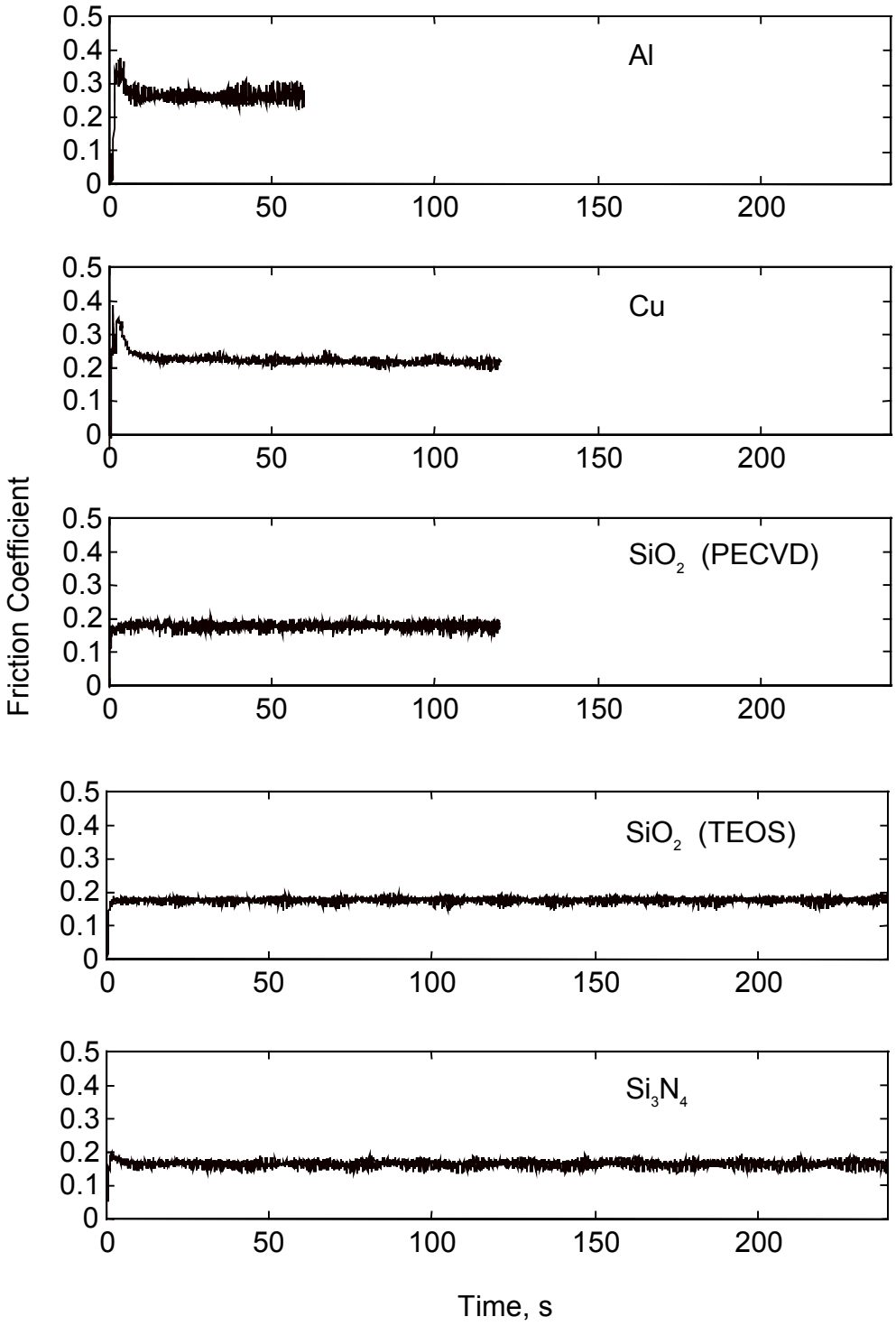

Figure 3.3 Friction coefficient versus time for various coatings: Buehler CHEMOMET pad, 300 nm abrasive.

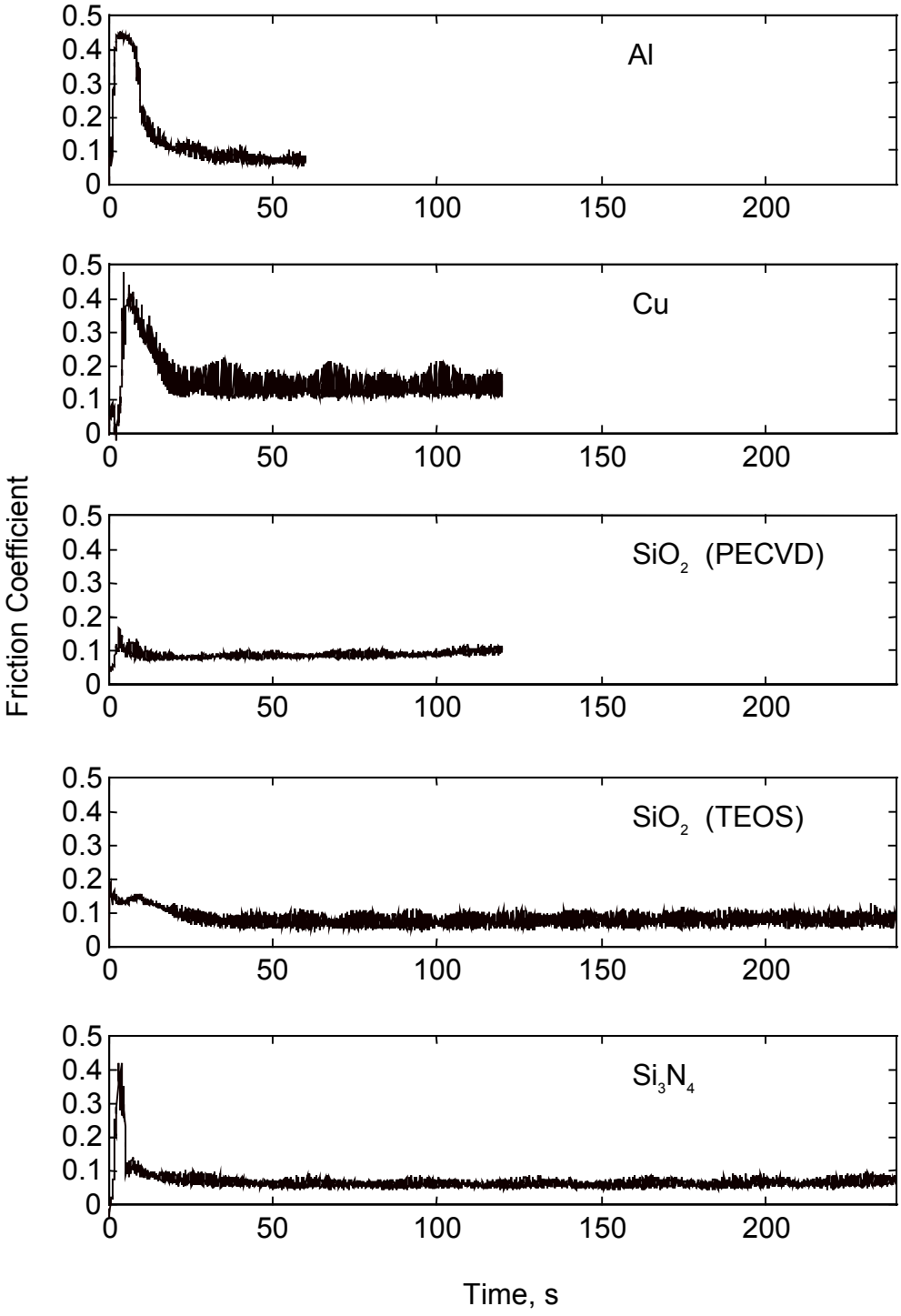

Figure 3.4 Friction coefficient versus time for various coatings: Rodel IC-1400 pad, 300 nm abrasive.

throughout the process. The initial high friction coefficient might be due to direct contact between the coating surface and the pad asperities without fully dispensed slurry. After a few seconds, the friction coefficient drops to a lower, steady value. The steady-state friction coefficient ranges from 0.15 to 0.28 on the Buehler pad, and from 0.09 to 0.17 on the Rodel pad for all coatings tested. According to Chapter 2, the friction coefficient of the order of 0.1 indicates that the wafer/pad interface is in the contact regime. For some experiments on the Rodel pad, the contact condition may have been close to the transition point to the mixed mode because the friction coefficient is slightly less than 0.1. The friction coefficient is slightly higher for Al and Cu and lower for SiO_2 and Si_3N_4. However, the difference is small, around 0.1 to 0.2, comparable to variations for the same material.

Tables 3.3 and 3.4 present the experimental results with Buehler and Rodel pads, including friction coefficient, mass loss, volume loss, material removal rate (MRR), normalized material removal rate (NMRR), Preston constant (k_p), and wear coefficient (k_w). Figure 3.5 shows the friction coefficient against the hardness of the coating materials. The friction coefficient and material hardness are not strongly correlated over a wide range of hardness. The friction coefficient is, however, consistently higher for soft materials like Al and is generally higher on the Buehler pad for all experimental coatings.

3.3.2 Material Removal. Figure 3.6 shows the effect of material hardness on material removal. The MRR, ranging from 330 nm/min to 4 nm/min, decreases with the increase in the hardness of the coating. The solid line is a linear least-square fit of the data for both pads on logarithmic scales. The slope of the line is about -1.155, which indicates that MRR is approximately inversely proportionate to the hardness of the coating. Additionally, both pads yield similar slopes, -1.147 for the Buehler pad and -1.164 for the Rodel pad. This implies that the wear coefficient of coatings is the same (Eq. (3.4)) because the same normal pressure and velocity were applied in all experiments. The intercepts of the lines with the abscissa at which hardness is 1 MPa are 5.739, 5.755 and 5.724 for overall data and for the Buehler and Rodel pads, respectively. Thus the MRR is 1.07 times greater on the Buehler pad. This is almost negligible considering the variation in the data. Figure 3.7 shows the effects of hardness on normalized material removal rate (NMRR). The plot is similar to Fig. 3.6

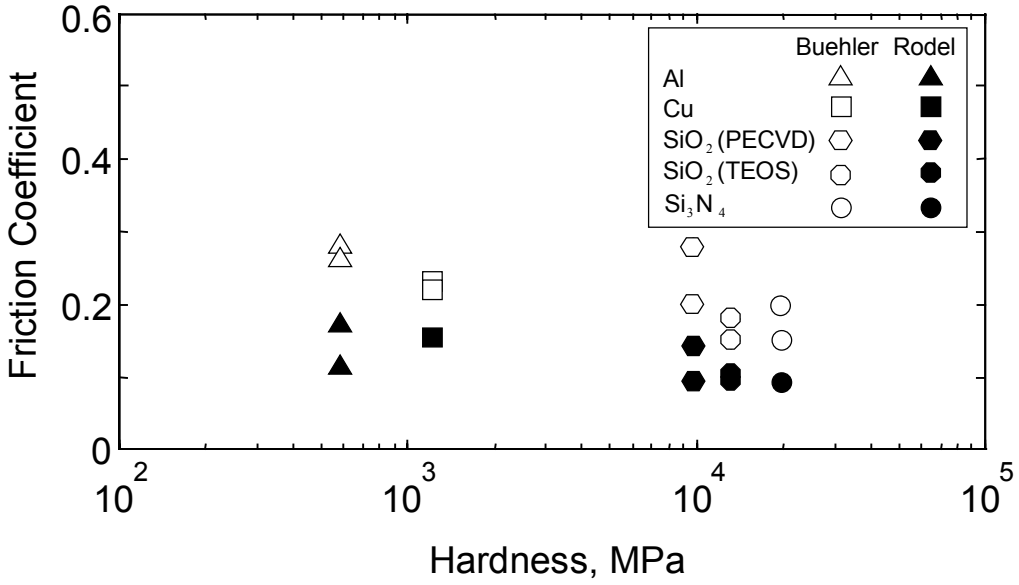

Figure 3.5 Effect of coating hardness on friction coefficient with 300 nm abrasive.

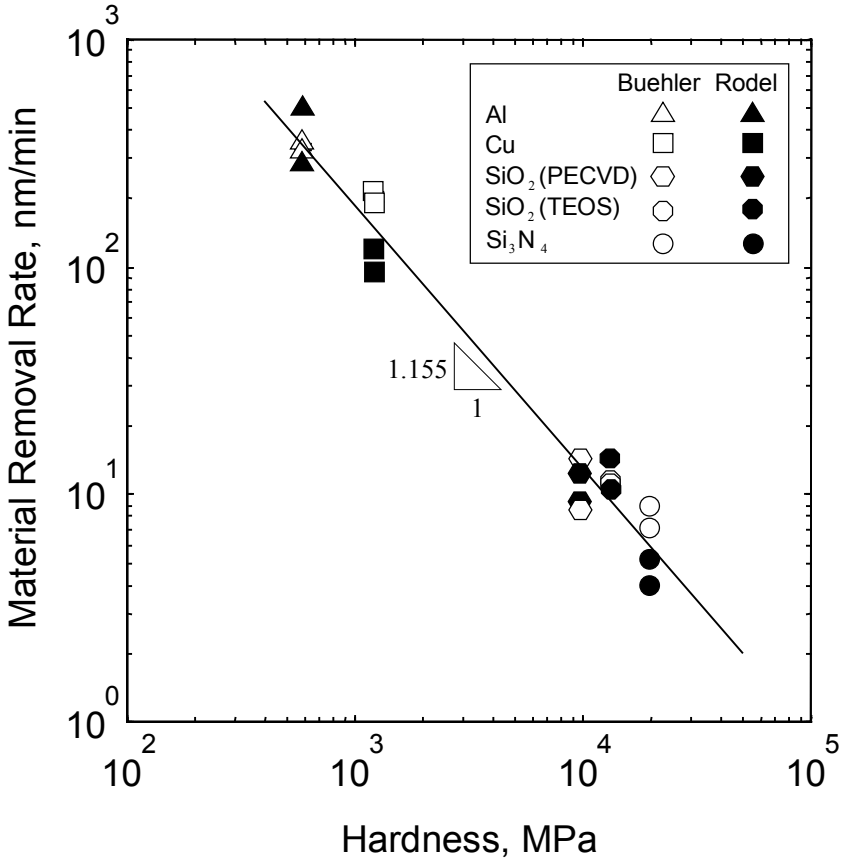

Figure 3.6 Effect of coating hardness on material removal rate with 300 nm abrasive.

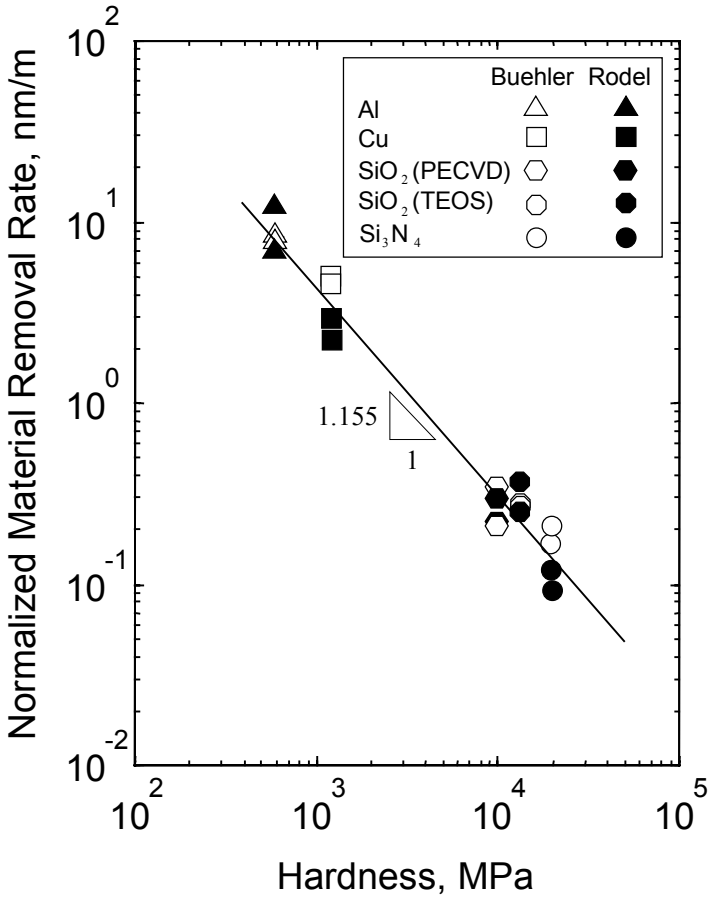

Figure 3.7 Effect of coating hardness on normalized material removal rate with 300 nm abrasive.

because the NMRR is defined as the MRR divided by the relative velocity, which is the same in all experiments. The NMRR ranges from 0.1 nm/m for Si_3N_4 to 10 nm/m for Al.

Based on the Preston Equation Eq. (3.1), the Preston constant is calculated and plotted against coating hardness in Fig. 3.8. The trend of the data and the slope of the linear least-squares fit are the same as those on the MRR plot because the normal pressure and relative velocity were the same in all experiments. Figure 3.9 shows the relation between the wear coefficient and coating hardness. There is no significant correlation between wear coefficient and hardness. This verifies the relation between the Preston constant and the wear coefficient given in Eq. (3.5). The wear coefficient is about 10^{-4} for all coatings. When compared to other wear situations such as 0.1 -1 in cutting process and 10^{-2}-10^{-1} in grinding, the much smaller wear coefficient in polishing indicates that not only the scale of material removal is smaller, but the mechanism(s) might be different. The detailed mechanism(s) of the material removal will be addressed in a later section.

Figure 3.10 is a MRR bar graph of the two different polishing pads. For each coating material, the Buehler pad seems to enhance MRR for both Al and Cu, about 1.2 and 1.9 times higher than that on the Rodel pad. However, there is almost no significant difference in MRR for both SiO_2 and Si_3N_4. Figure 3.10 further emphasizes the great difference of MRR between metals and ceramics which must be addressed in metal-patterned wafer polishing.

3.3.3 Within-Wafer Nonuniformity. The MRR reported above is an average value, i.e., the coating material is assumed to be removed uniformly across the wafer and thus the thickness reduction rate can be calculated directly from the volume loss. However, the material removal rate actually may vary across the wafer due to the non-uniform pressure distribution on the wafer surface or due to the pad compliance. Figure 3.11 shows examples of pad stiffness on the PECVD SiO_2 thickness variation across the wafer. The within-wafer nonuniformity (WIWNU) increased slightly, from 0.78% to 1.00%, on the Buehler pad and decreased slightly, from 0.81% to 0.76 %, on the Rodel pad after 2 minutes of polishing. Table 3.5 compares WIWNU before and after polishing on Rodel pads for SiO_2 and Si_3N_4.

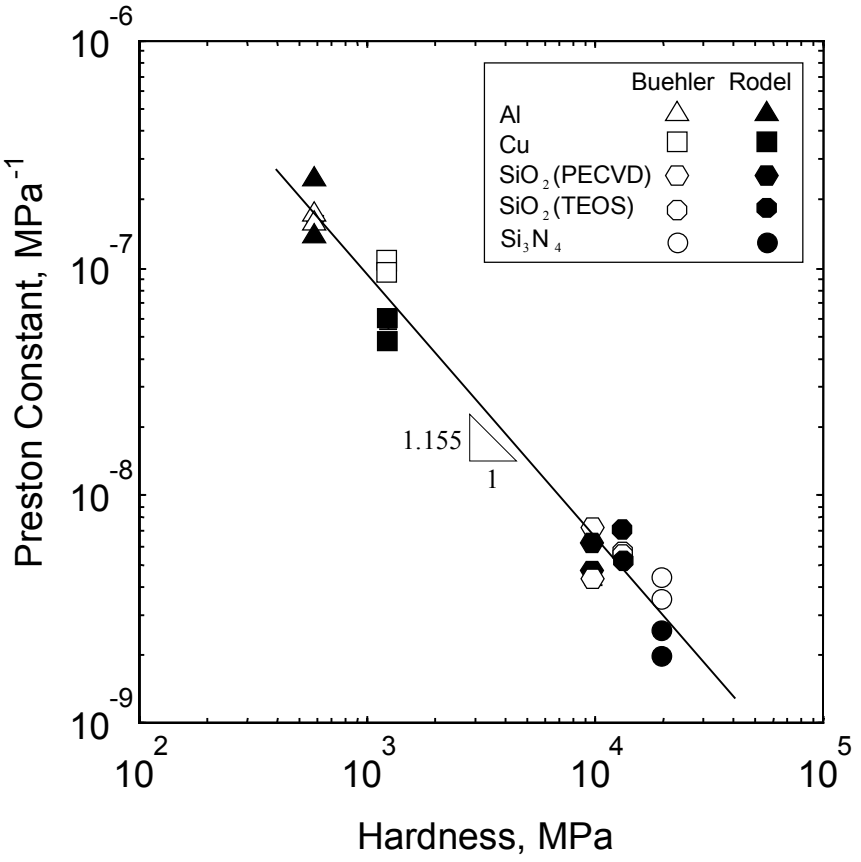

Figure 3.8 Effect of coating hardness on Preston constant with 300 nm abrasive.

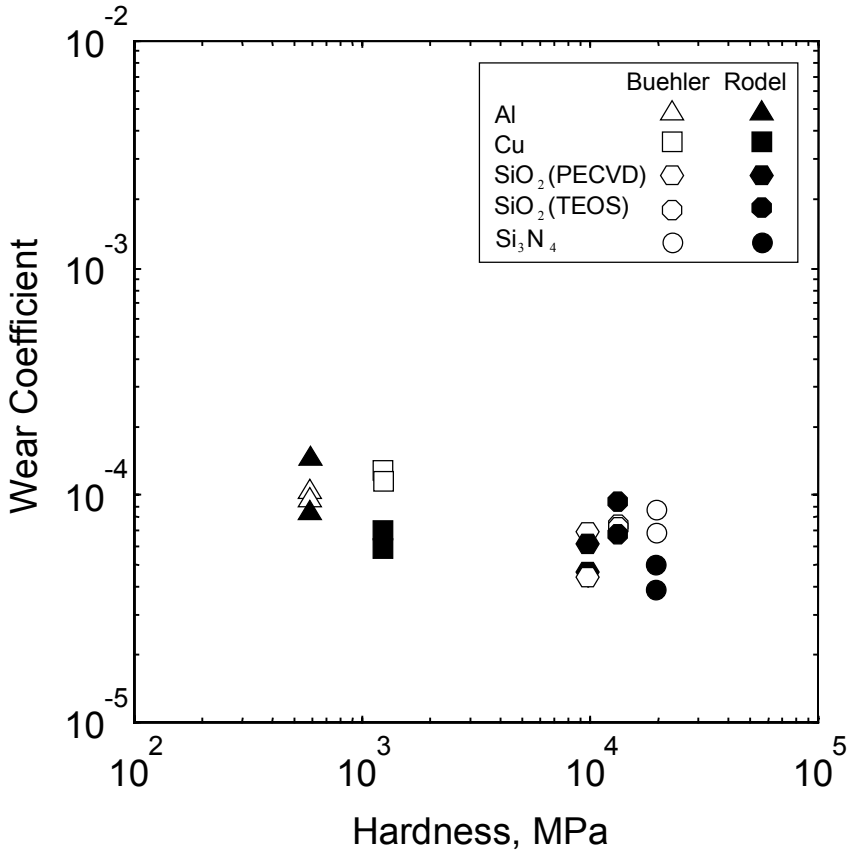

Figure 3.9 Effects material hardness on wear coefficient for experimental pads with 300 nm abrasives.

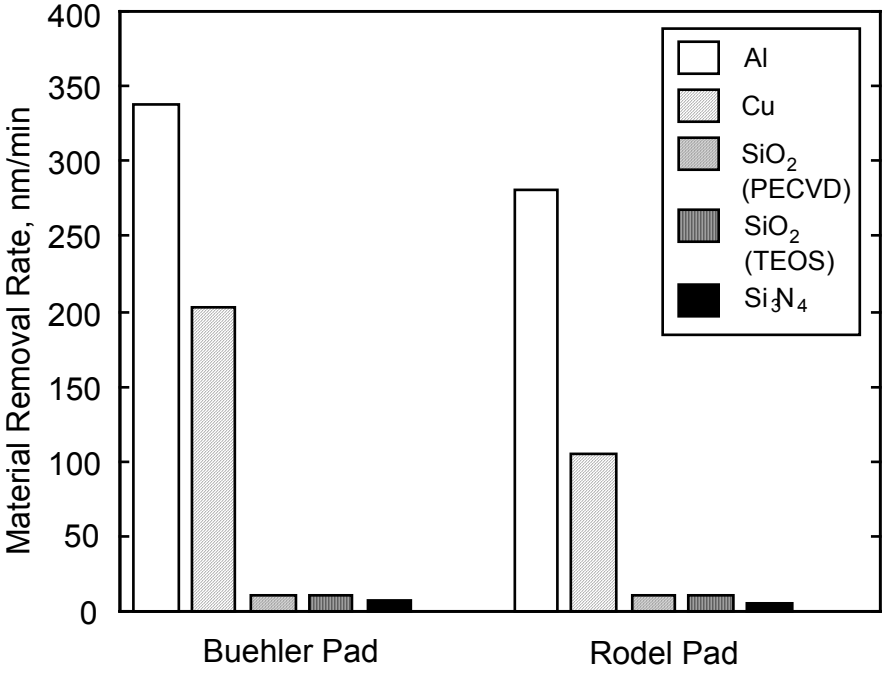

Figure 3.10 Comparison of material removal rates of various coatings: Buehler and Rodel pads with 300 nm abrasive.

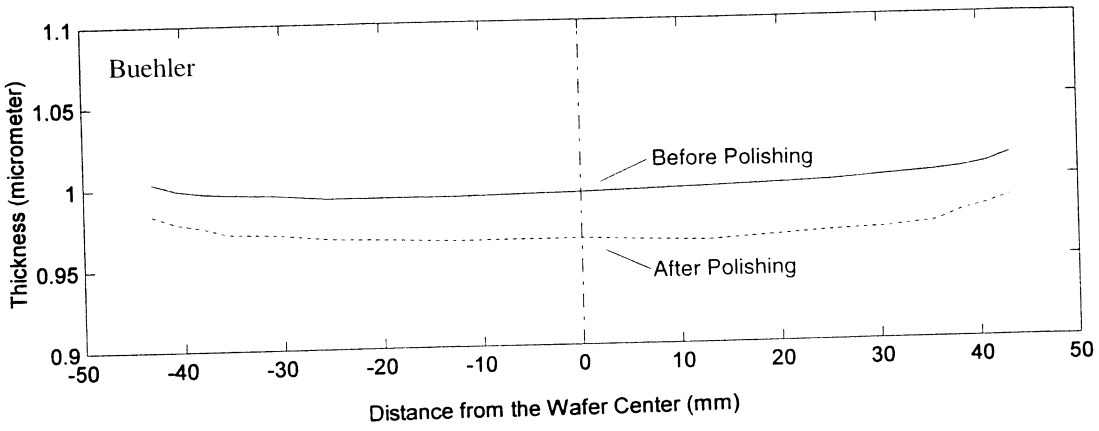

(a)

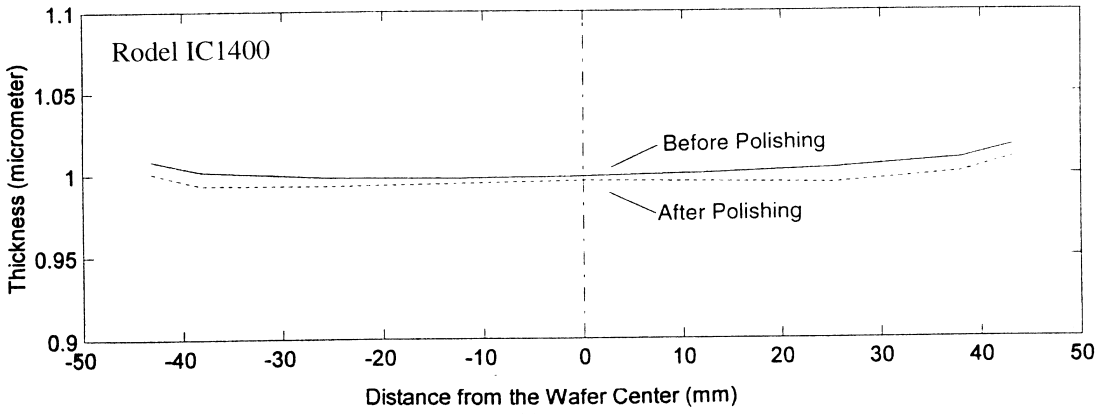

(b)

Figure 3.11 Thickness variation of the PECVD SiO_2 coating across the wafer: after polishing on (a) Buehler CHEMOMET pad and (b) Rodel IC-1400 pad. The solid and dashed lines represent the thickness before and after polishing, respectively

Table 3.5: Within-wafer nonuniformity (WIWNU) before and after polishing on Rodel pad.

Coating	Before Polishing WIWNU (%)	After Polishing WIWNU (%)
SiO_2 (PECVD)	0.81	0.76
SiO_2 (TEOS)	1.20	2.32
Si_3N_4	0.56	0.80

* Abrasive: 300 nm α-Al_2O_3 .

3.3.4 Surface Roughness and Scratches. Figure 3.12 is a SEM micrograph of the surface of a Cu wafer after polishing on a Rodel pad. There are two major effects from the abrasive action in polishing: defects like scratches and pits and increased surface roughness. Figure 3.13 shows the AFM micrographs of a Cu surface on a 5μm x 5μm area near the wafer center before and after polishing with 50 nm, 300 nm, and 1000 nm abrasives, respectively. Figure 3.13 (a) shows a spotty microstructure on the Cu wafer surface after sputtering. After polishing, the initial structure is removed and many fine grooves and a few deep, big scratches were observed on the surface. Deep and wide scratches were found on the Cu surface polished with larger size abrasives. Moreover, neither wear debris nor wedges were found on the surface. Therefore, the grooves might be primarily formed by slight plowing due to the repeated loading and sliding of abrasive particles.

Three statistics from the three-dimensional profile data were obtained to characterize the surface. The mean roughness, R_a, and the root-mean-square (RMS) roughness, R_q, represent the surface roughness, and the maximum roughness, R_z, the depth of the scratches. For all three abrasive sizes, R_a, R_q, and R_z increase after polishing on the Cu wafers. Both R_a and R_q increase slightly with the abrasive size, about 1.6 times for 20 times increase in abrasive size. However, R_z increases about 2.3 times with the abrasive size from 50 nm to 300 nm, but barely changes for 300 nm to 1000 nm. Figure 3.14 shows the cross-sections of the surface scans. The deep grooves increase both in number and depth with the increase of abrasive size. This means that the scratch density and depth increase with the abrasive size. Table 3.6 summarizes the effects of abrasive size on Cu wafers. The material removal rate on Cu wafers increases about 2.2 times when the particle size increases from 50 nm to 300 nm, and 1.2 times more when the size is further increased to 1000 nm. However, increased particle size does not increase R_a and R_q. The important effect of increasing abrasive size on surface characteristics is to increase the scratch size and density.

Table 3.7 lists the surface roughness of various surface coatings before and after polishing on the Rodel pad with 300 nm abrasive slurry. The mean and RMS roughnesses for both metals and ceramics remain low afer polishing. Nevertheless, the maximum roughness increases about six and three times on Al and Cu, respectively, while increasing less than one

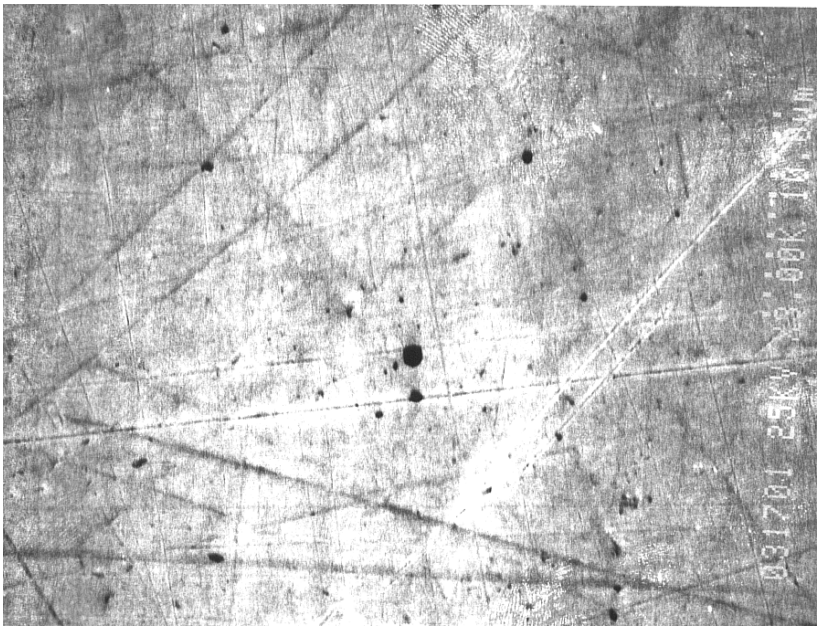

Figure 3.12 SEM micrograph of a Cu-coated wafer surface after polishing.

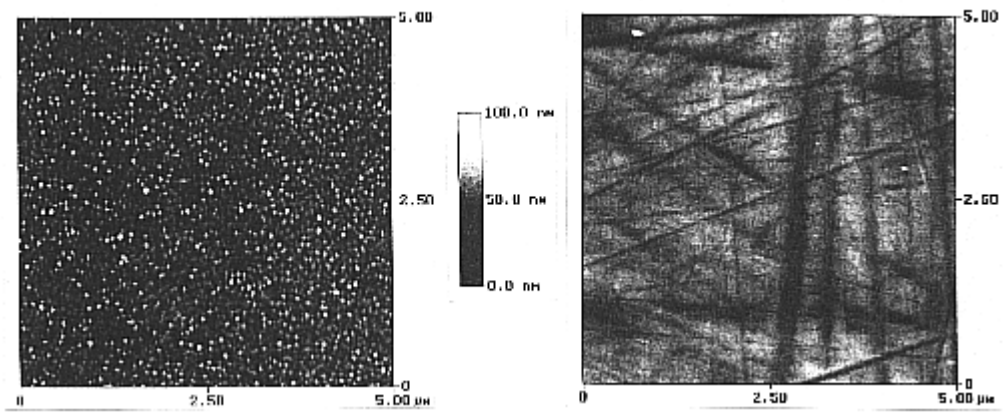

(a) (b)

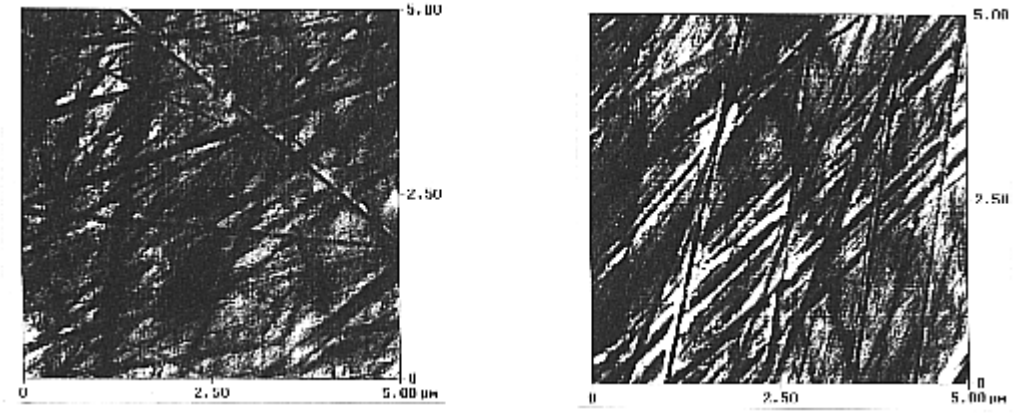

(c) (d)

Figure 3.13 AFM micrographs of Cu surfaces (a) before polishing (R_a= 3.7 nm, R_q= 4.6 nm, and R_z= 35.1 nm), (b) polished with 50 nm abrasives (R_a= 3.8 nm, R_q= 4.8 nm, and R_z= 41.6 nm), (c) polished with 300 nm abrasives (R_a= 4.0 nm, R_q= 5.7 nm, and R_z= 98.2 nm), and (d) polished with 1000 nm abrasives (R_a= 6.0 nm, R_q= 7.9 nm, and R_z= 85.4 nm).

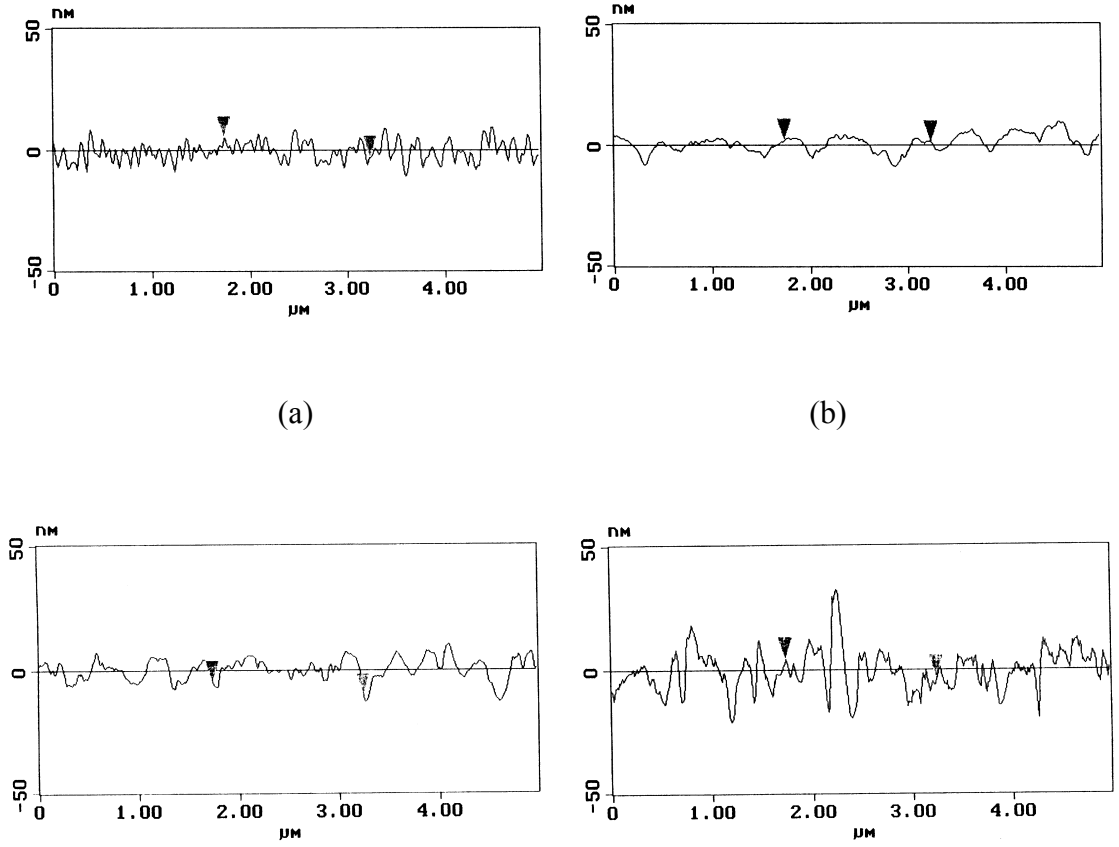

Figure 3.14 AFM micrographs of corss-sections of Cu surfaces: (a) before polishing (R_a= 3.7 nm, R_q= 4.6 nm, and R_z= 35.1 nm), (b) polished with 50 nm abrasives (R_a= 4.0 nm, R_q= 4.9 nm, and R_z= 17.5 nm), (c) polished with 300 nm abrasives (R_a= 2.5 nm, R_q= 3.3 nm, and R_z= 8.1 nm), and (d) polished with 1000 nm abrasives (R_a= 7.1 nm, R_q= 10.4 nm, and R_z= 50.6 nm).

Table 3.6: Abrasive size effects in copper polishing.

Particle Size (nm)	MRR (nm/min)	Surface Roughness R_a (nm)	R_q (nm)	R_z (nm)
50	51	3.8	4.8	41.6
300	112	4.0	5.7	98.2
1,000	133	6.1	7.9	85.4

and a half times on SiO_2 and Si_3N_4. Figure 3.15 shows that the surface roughness and scratches are affected by the pad stiffness for Cu samples. The mean and RMS roughnesses are not affected by the pad used. However, the maximum roughness seems to correlate with the pad stiffness. The stiffer the pad, the higher the R_z.

3.4 Discussion

Several models of polishing have been proposed over the decades. They include: surface melting, brittle fracture, microcutting, and burnishing. Each model emphasizes some fundamental mechanism of polishing and attempts to explain the phenomenon of material removal. Because many variables are involved in polishing (e.g., materials, pressure and velocity on the specimen, polishing pads, and abrasive), a single mechanism cannot explain all aspects of polishing. Nevertheless, the following sections review several analytical models to elucidate the effects of certain process parameters on friction, material removal, and topography of polished surfaces. The present experimental results on wafer polishing are examined in light of these models.

3.4.1 Surface Melting. When two surfaces slide relatively, most of the work done is converted into heat. In polishing, the heat is generated at the particle/surface contact area, a small fraction of the nominal area, and mostly diffuses through those contacts. A much higher temperature rise, or flash temperature, is expected at those contacts than in the bulk and may be sufficient to soften or even melt the surface. Many polishing situations create a thin, amorphous layer. Some researchers attribute this phenomenon to the rapid solidification of the melt (Bowden and Hughes, 1937). Wear occurs when the softened or melted material is smeared over the surface and eventually comes off the interface. The flash temperature T_f depends on the geometry of particle/wafer contacting area and the thermal conductivities of the sliding surfaces. In the steady state, T_f can be expressed as (Jaeger, 1942; Bowden and Tabor, 1950; see Appendix A):

$$T_f = T_o + \frac{\mu f_n v_R}{2w} \frac{1}{k_1 + k_2} \tag{3.3}$$

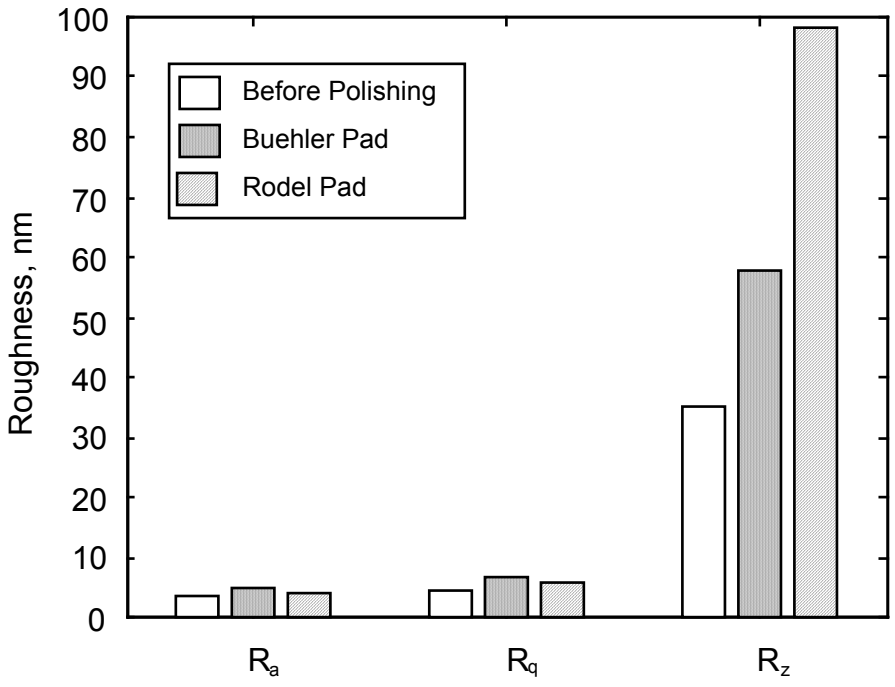

Figure 3.15 Surface roughness of Cu coatings polished with 300 nm abrasive.

where T_o is the bulk temperature far away from the contact, μ the friction coefficient, f_n the normal load on the abrasive, v_R the relative sliding velocity, w radius of the circular contact region of a spherical abrasive particle, and k_1 and k_2 are the thermal conductivities of the coating material and the particle, respectively.

The bulk temperature can be assumed to be the room temperature, since the polishing period is short and the back sides of the wafer and the pad are sometimes cooled. If it is assumed that heat transfer into the particle/pad side is negligible, since the thermal conductivity of Al_2O_3 is much smaller than the metallic coatings, Cu and Al, the flash temperature can be estimated by Eq. (3.3). The friction coefficient and the width of the contacting area are about 0.15 and 80 nm for Cu polishing with 300 nm Al_2O_3. As shown later, the normal load on a particles is about $6x10^{-6}$ N. Using these data, the increase of flash temperature (T_f - T_o) for Cu polishing is estimated to be $6.5x10^{-3}$ K, thus melting is unlikely. Melting is even less likely for ceramic coatings because of the much higher melting point of those materials. In fact, the flash temperature in the CMP conditions will stay low because of the low sliding velocity, the light load applied on the small abrasive, and the low friction coefficient due to the presence of slurry.

The removal of material from the coating surface in the melting mode requires both that the flash temperature reaches the melting temperature and the melt form hot wear particles or a molten stream which will be consequently ejected form the interface (Lim and Ashby, 1986). Although bulk temperature may rise with continued polishing, the circulation of slurry at the contact interface will remove a larger part of the heat generated to keep the bulk temperature far below the melting point. Therefore, even if the flash temperature reaches the melting point, the melt will flow to the surrounding cool surface, to resolidify without generating hot wear particles or squirting out as a molten stream. It may be concluded therefore that under typical CMP conditions, material removal by melting is not a viable mechanism.

3.4.2 Microcutting. In this polishing mode, abrasive particles act as single-point cutting tools and produce shallower and narrower grooves than those in grinding or other abrasion processes. Hardness determines the depth of particle penetration and, therefore, the MRR and surface finish. The abrasive is normally harder than the surface being polished to maintain a

high rate of material removal. The frictional force is mostly due to the resistance of the soft surface being polished to plastic flow. Upper bound estimates for the friction coefficient and for material removal rate in the microcutting mode have been made in the past by idealizing the shape of the abrasive tip as a cone or a sphere (Goddard and Wilman, 1962; Sin et al., 1979; Komvopoulos et al., 1984).

For a conical tip of abrasive particle, the friction coefficient μ, the wear coefficient k_w, and surface roughness R_a due to microcutting can be written as (see Appendix B):

$$\mu = \frac{2}{\pi}\left(\tan\theta + \frac{s}{H}\sec\theta\right) \tag{3.4}$$

$$k_w = \frac{VH}{LS} = \frac{\tan\theta}{2\pi} \tag{3.5}$$

$$R_a \approx \frac{d}{2} = \frac{w}{4}\tan\theta \tag{3.6}$$

where d is the depth of the grooves, w the width of the grooves, θ the angle between the abrasive and the surface, s the interfacial shear stress due to adhesion, and H the hardness of the coating. Since the abrasive particle is so small, θ cannot be specified a priori. An alternative is to measure the groove angle to estimate θ. Based on experimental results, for example, Cu wafers with 300 nm Al_2O_3 abrasive particles, $w \approx 80$ nm and $\theta \approx 9°$. The friction coefficient and the wear coefficient calculated by Eqs. (3.4) and (3.5) are 0.10 and 0.025, respectively. In this calculation and the following case, the adhesion shear stress s is assumed to be negligible due to the presence of slurry at the contacting interface as a contaminant.

Similarly, for a spherical tip, which is closer to the shape of the abrasive particles, the friction coefficient, wear coefficient and surface roughness can be expressed as:

$$\mu = \frac{2}{\pi}\left(\frac{2r}{w}\right)^2\left\{\sin^{-1}\frac{w}{2r} - \frac{w}{2r}\left[1-\left(\frac{w}{2r}\right)^2\right]^{1/2}\right\} + 2\frac{s}{H}\left\{1-\left[1-\left(\frac{w}{2r}\right)^2\right]^{1/2}\right\} \tag{3.7}$$

$$k_w = \frac{2}{\pi}\left(\frac{2r}{w}\right)^2 \left\{ \sin^{-1}\left(\frac{w}{2r}\right) - \left(\frac{w}{2r}\right) + \frac{1}{2}\left(\frac{w}{2r}\right)^3 \right\} \tag{3.8}$$

$$R_a \approx \frac{d}{2} = \frac{f_n}{2\pi r H} \tag{3.9}$$

Substituting the measured values of w and r in Eqs. (3.7) and (3.8), μ and k_w are estimated to be 0.12 and 0.11, respectively. The friction coefficients, predicted by the microcutting model, for either cone or spherical abrasive, is close to the experimental values, about 0.15 - 0.22 for Cu. This suggests that the microcutting model explains, in part at least, the transmission of normal and shear stresses due to the action of the abrasive particle on the coating on a local scale. On the other hand, the estimated wear coefficient by the microcutting model, which ranges between 10^{-2} and 10^{-1}, is two to three orders of magnitude higher than the experimental results $\approx 10^{-4}$. The much smaller material removal implies that the material was not cleanly sheared off by a single pass of the abrasive particle. This point is also supported by the observation that no chip-like wear particles were found on the worn wafer or post-CMP pad surfaces. Instead, ridges were formed along with some deeper and wider grooves, which suggests particle plowing. In fact, early research in abrasive wear (Sin et al., 1979) found that when the attack angle θ between the abrasive and the coating surface is small (i.e. the rake angle is a large negative value) large plastic deformation occurs at the surface and in the subsurface region below the contact. Since the penetration depth in the CMP condition is usually very shallow, the attack angle for any shape of particles will be very small. Therefore, it is more likely that plowing will prevail rather than cutting. Similar results were reported by Hokkirigawa and Kato (1988).

The smaller k_w also suggests that much of the work done by abrasive particles on the coating is to plastically deform the subsurface. The wear equation, Eq. (3.2), can be rewritten as (Suh, 1986):

$$k_w = \frac{VH}{LS} = \mu \frac{VH}{\mu LS} = \frac{Vu}{FS} \tag{3.10}$$

where F is the tangential force on the wafer and u the specific energy, the work done to remove a unit volume of material. If cutting without plastic deformation is presumed, i.e. the plastic zone is limited to the grooved region, the specific energy is approximately equal to the hardness of the material being polished. Thus, based on Eq. (3.10), the wear coefficient can be interpreted as the ratio of work done by creating chips by cutting ($=Vu$) to the total external work done ($=FS$). When cutting is the dominant mechanism, most of energy is consumed to create chips and k_w should be close to unity. Because k_w is much less than unity in polishing, most of the external work is dissipated into the sub-surface region below the contact to create a large plastic deformation zone, deeper than the dimension of the grooves.

For these reasons, the microcutting model grossly overestimates the MRR. Nevertheless, for delineating the effects of important process parameters on the friction coefficient, wear coefficient, and surface roughness, the previous analysis is adequate to provide a qualitative picture of the polishing process. Moreover, from Eq. (3.9), the average load supported by a single abrasive particle is estimated to be about 6 μN.

3.4.3 Brittle Fracture. Fracture by plastic indentation occurs in brittle materials such as glass when the tip radius of the abrasive particle is below a critical value. In this small-scale contact, cracks are not induced in the elastic loading regime, but are observed with elastic/plastic penetration of particles. Lateral cracks initiate when the medium is unloaded. They propagate parallel to the surface with repeat loading/unloading and finally reach the surface to form wear particles. Cracks initiate when the load on the particle exceeds a transition threshold, f_n^* (Evans and Marshall, 1980):

$$f_n^* = \kappa \left(\frac{K_c^4}{H^3} \right) f(E/H) \tag{3.11}$$

where κ is a dimensionless constant, K_c the fracture toughness, H the hardness, and E the Young's modulus of the material being polished. For lateral cracks, $f(E/H)$ varies slowly with E/H and $\kappa f(E/H)$ is approximately 2×10^5. Table 3.8 presents the toughness and hardness of the typical wafer coatings and their predicted critical loads. The critical load for both metal and ceramic coatings is many orders of magnitude greater than the load estimated earlier by

particle penetration measurement, about 10^{-6} N for a typical CMP with 300 nm abrasive particles. Therefore, the small particles employed in CMP generally prevent the initiation of cracks and the subsequent fracture. This again suggests that the prevailing mechanism of material removal is excessive plastic deformation.

In addition, the smallest particle size r^* to induce brittle fracture, especially for brittle coating materials like SiO_2 and Si_3N_4, can be estimated by the relation of plastic indentation.

$$H = \frac{f_n^*}{\pi r^{*}} \tag{3.12}$$

When the radius of the abrasive is smaller than r^*, the average pressure applied on the particle is greater than the resistance of the material to plastic flow, or the hardness. Thus, plastic deformation will determine the material removal before the cracks initiate. If the radius of the abrasive is larger than r^*, cracks may be able to initiate and develop in the subsurface and dominate the rate of material removal. Table 3.8 lists the calculation results of r^*. For metals, the fracture mechanism is ruled out because of the high toughness and low hardness. Even for SiO_2 and Si_3N_4, the critical particle size r^* is one to two orders of magnitude greater than the size used in CMP.

In any case, the fracture mode of material removal is generally not accountable in the CMP process. The larger size of particles required to initiate fracture will create deeper and wider grooves on the surface. The lateral fracture depth is on the same scale as the plastic zone radius, which is usually much deeper than the plastic grooves. Although the MRR is expected to be higher, the increase of the surface roughness (due to plastic penetration) and the generation of large surface scratches (due to brittle wear tracks) are obviously unacceptable in the sub-micron semiconductor fabrication environment.

3.4.4 Burnishing. Burnish, in which material is removed on a molecular scale, represents the least possible amount of wear. The wear coefficient can be as small as 10^{-8}. The mechanisms of burnish are not yet clear. There is no direct observation to verify the hypothesis. It is proposed that material is removed molecule by molecule from the high spots

Table 3.8: Estimates of the threshold load and the critical size for lateral crack initiation.

Material	Toughness, K_c (MPa$\sqrt{m}$)	Hardness, H (MPa)	K_c^4/H^3 (N)	f_n^* (N)	r^* (μm)
Al	140	591	1.86×10^6	3.72×10^{11}	2.83×10^6
Cu	110	1,220	8.06×10^4	1.22×10^{10}	4.10×10^6
SiO_2	0.7	9,793	2.55×10^{-7}	5.10×10^{-2}	2.58
Si_3N_4	5.5	19,580	1.22×10^{-4}	2.44×10^1	39.80

by adhesive forces between the abrasive and surface material when the load is below a critical value. Therefore, the surface topography due to burnishing will be as smooth as that produced by evaporation. For a single-point contact system (like pin-on-disk), the critical load below which burnish might prevail is given by (Rabinowicz, 1968):

$$L = 10^8 \pi \frac{W_{ab}^2}{H} \tag{3.13}$$

where L is the normal load and W_{ab} (= $\gamma_a+\gamma_b-\gamma_{ab}$) the surface energy of adhesion. For Cu polishing with Al_2O_3, γ_a (Al_2O_3) is 590 erg/cm^2, γ_b (Cu) 1120 erg/cm^2, and γ_{ab} assumed to be zero since the presence of slurry at the interface. Thus, L must be lower than 0.74 N for burnishing based on Eq. (3.13). Nevertheless, Eq. (3.13) is reasonably obeyed, especially for noble metal contacts, but not widely tested for other materials. On the other hand, the wear coefficient reported for burnishing is about 10^{-8}, which is far below k_w, about 10^{-4}, in the polishing experiments. It suggests that burnishing, even if it occurs, is not the dominant material removal mechanism under CMP conditions.

The above analyses reviewed several polishing models based on the experimental results. Material removal due to plastic deformation of the coating reasonably explains the genesis of friction and the formation of grooves and scratches in polishing. However, the estimate of the wear coefficient by the microcutting assumption, as the upper bound for plastic deformation model, is two orders of magnitude greater than those of the experiments. The discrepancy was explained earlier by the abrasive plowing which creates a deeper plastic deformation zone in the subsurface than the depth of the surface groove without cutting out the surface material. The surface material will remain mostly in the groove to form ridges along the side of the groove. Thus k_w is much smaller than that estimated by the microcutting model.

There are other possibilities to explain the low wear coefficient. In reality, the load applied on the wafer is carried both by the wafer/particle and by the wafer/pad contacts. In the previous analyses, the elastic/plastic deformation of the pad was not considered and the load was assumed to be carried by the particles only. However, about $7x10^7$ particles are needed to carry all the load, many fewer than the number of particles needed to cover the 100 mm wafer

surface, about 10^{11}, closely packed. On the other hand, the particle size employed in a CMP, about 150 - 300 nm nominally, is comparable or smaller than the surface roughness of the pad surface. The pad is much softer, approximately E = 0.5 GPa for the IC-1000 top pad, than the abrasive and coating materials, approximately E = 120 GPa and H = 1220 MPa for Cu. Therefore, the abrasive will embed in the pad surface and increase the wafer/pad contact area.

Figure 3.16 presents evidence for wafer/pad direct contact. A flattened, plastically deformed pad surface analyzed after polishing 20 wafers without conditioning indicates that the pad has been in contact with flat wafer surface and carries load in polishing. Because the pad is much softer than the coating, there is essentially no material removal at the wafer/pad contact regions. Hence, k_w estimated by Eq. (3.2) based on the total load on the wafer will be smaller than that by Eq. (3.8). Pad/wafer contacts not only decrease k_w, but also increase the total frictional force due to the higher friction coefficient at the wafer/pad interface. This is shown by the increase on friction coefficient in experiments, from the estimated values 0.1 - 0.15 to experimental values up to 0.28.

Another factor resulting in a smaller k_w is that the abrasive particles roll rather than slide at the contact interface. The friction coefficient of the rolling contact usually is much smaller, lower than 0.1, than that of the sliding contact, about 0.1 - 0.15, although the same load is carried by the particle. The total frictional force might be written approximately as the weighted sum of the frictional forces due to the particle sliding contact, rolling contact and the wafer/pad contact. The smaller frictional coefficient for the particle rolling contact offsets the high friction, about 0.5 -0.7, at the wafer/pad contact. Consequently, the overall friction coefficient still remains at a lower level, about 0.1 - 0.3. Due to the particle rolling, the volume of material removed is not proportional to sliding distance and results in an overestimate on k_w in both Eqs. (3.2) and (3.8).

Based on Eq. (3.8), the wear coefficient k_w depends on the ratio of particle penetration width to particle radius. For a small k_w, the equation implies that the radius of the particle employed at the polishing interface might be larger than the nominal size because the penetration width is a measured value. This may be due to the agglomeration of the small abrasive particles to reduce the surface energy. Another possibility is related to the pad

porous macrostructure. The surface pores, ranging from 2 - 5 μm to 50 - 80 μm, play an important role in collecting the worn abrasive and wear particles, retaining the slurry, and enhancing the local slurry dispensing. As shown in Fig. 3.17, the particles might easily fill up the small pores. Then the whole aggregate of particles acts like a large-radius cutting/plowing tool. When the pore size or the size of particle agglomerates has a broad distribution, the majority of the load is carried by a few, larger particles. The material removal rate and k_w will decrease with the decrease of active particles engaged in material removal (Bulsara et al., 1998). The size of surface grooves therefore will also present a wide range of distribution. Some large size scratches might appear on the polished surface, as shown in Figs. 3.12 and 3.13.

3.4.5. Process Optimization. The objectives of process optimization are to increase the MRR, k_p or k_w, and at the same time to maintain a low level of WIWNU and surface roughness and reduce surface scratching. From Eq. (3.1), the MRR increases with the pv_R. Based on the results presented in Chapter 2, the v_R/p ratio should be chosen so the wafer/pad interfacial condition remains in the contact regime. Heat generation and the WIWNU specification constraint the optimal pv_R product. Thus the key to enhance MRR is to increase the k_p or k_w.

Comparing theoretical estimates and experimental results, the two-orders-of-magnitude gap of k_w provides an opportunity for process improvement: it might be possible to increase the k_w without a significant increase of surface roughness by encouraging the mode of material removal from plowing toward microcutting. As discussed earlier, a larger size of particle can be employed to increase the k_w. However, the tradeoff of using larger abrasive is increased surface roughness and scratch size and density. A criterion to specify the surface roughness, usually 1/10 of the depth-of-focus of the lithography optics of about 20 nm for the current generation of technology, can be set such that a optimal particle size can be determined to yield a high k_w and a tolerable level of R_a and R_q. Results from the preliminary experiments on 50 nm, 300 nm, and 1000 nm dia. particles, summarized in Table 6, are in agreement with this optimization scheme, as shown in Fig. 3.18. The MRR, or k_w in this case

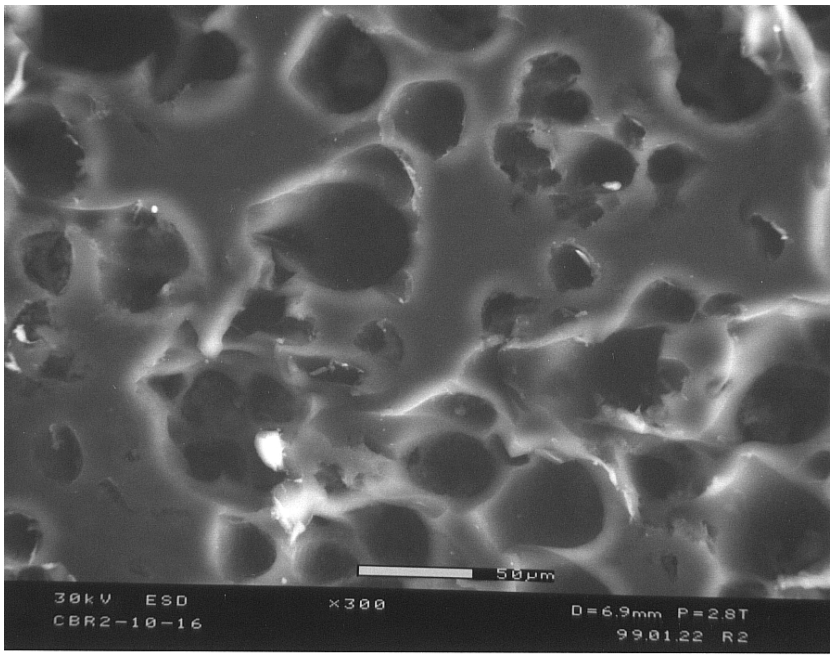

Figure 3.16 SEM micrograph of the plastically deformed Rodel IC-1400 pad after polishing.

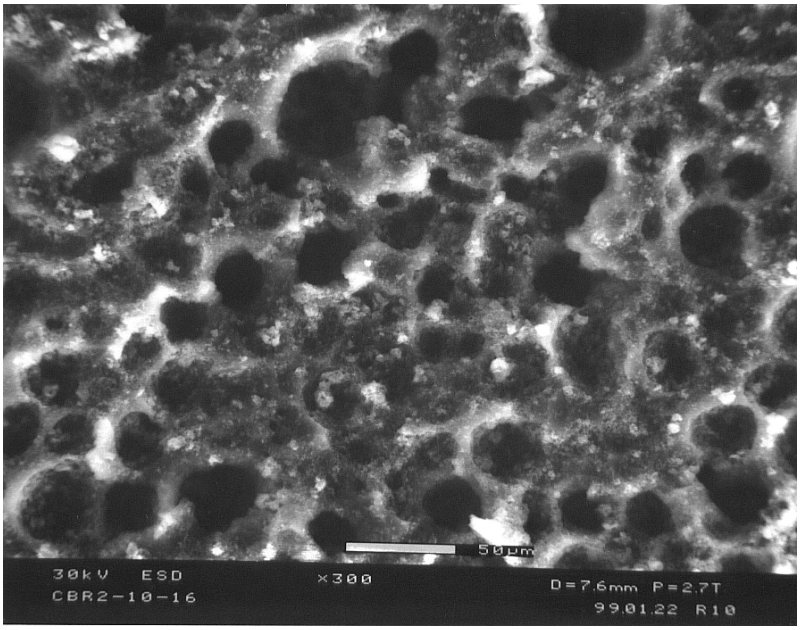

Figure 3.17 SEM micrograph of the dried post-polishing Rodel IC-1400 pad with slurry particles.

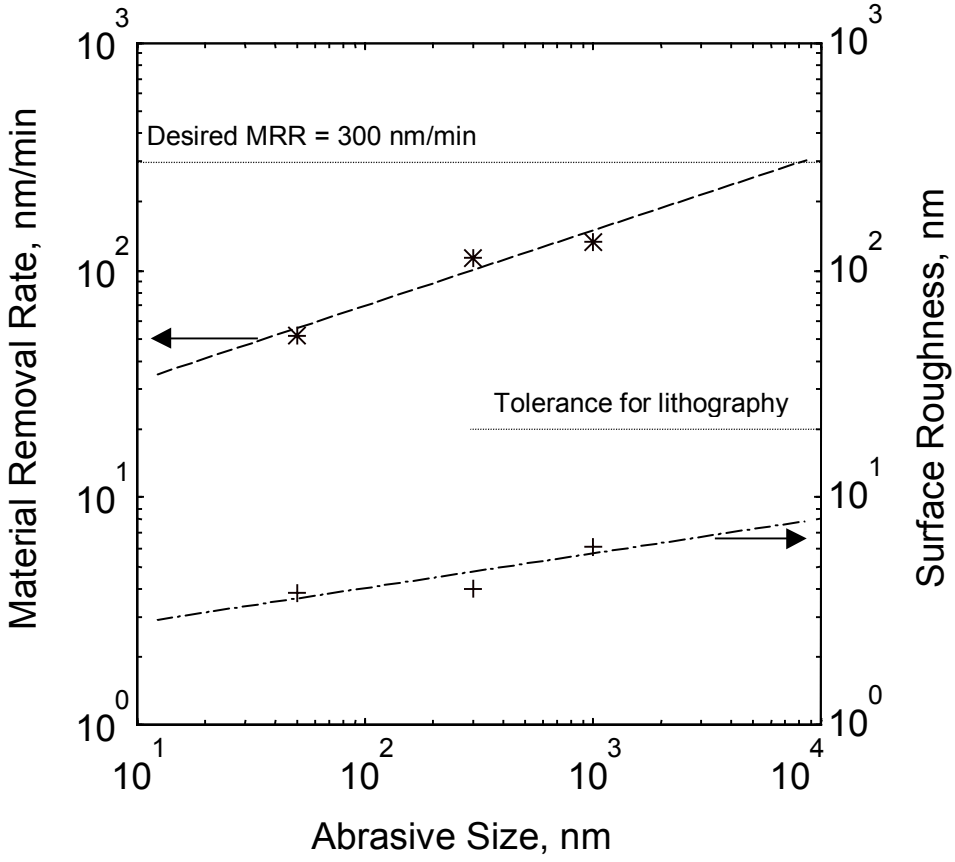

Figure 3.18 Process optimization scheme by emploing the abrasive size effect (on Cu wafers) .

due to the constant pv_R, increases about 2.6 times whereas the roughness remains at a low level when the particle size is increased from 50 nm to 1000 nm. Even larger particles might be employed in the future to find the optimal size. In addition, the pH value of the slurry can be adjusted to lift the MRR curve in Fig. 18 for specific material. The MRR of SiO_2 increases dramatically at pH values higher than 11. The MRR of Cu can be enhanced at a moderate acidic slurry, around 4 (Cook, 1990; Luo et al., 1998). It is believed that changing pH value will change the hardness of the coating to affect the MRR and k_w. On the other hand, the surface roughness is expected to remain at a low level, perhaps with a slight increase, in the chemical slurry with the same abrasive size because the load on the abrasive particles and the motion of particles at the wafer/pad interface are not affected by the chemicals. The scratch size and density also increase with particle size. A few big scratches, about 30 - 50 nm deep, were found in the Cu polishing. The larger scratches are due to the particle agglomeration and the high-end of the wide abrasive size distribution. In practice, some chemical agents might be added in the slurry to disperse the abrasive particles and prevent their agglomeration. The abrasive with a narrow peak size distribution (small standard deviation on the particle size distribution) can also reduce scratches.

Another scheme to increase k_w relies on preventing particle rolling, in which the particle/pad interfacial friction coefficient and the contact area must increase. The frictional coefficient between the abrasive particle and the pad depends on the adhesion of those two materials. The particle/pad contact area at a given load can be increased by choosing a soft pad material. However, according to the previous analyses, the decrease of pad hardness will increase the wafer/pad contact area and reduce the load distributed on the particle, thus reducing k_w. An appropriate pad material with good adhesion to abrasive particles, or even like lapping paper with fixed abrasive, with a sufficient hard surface layer might be used to increase the sliding and the load distributed on the particles to increase MRR and k_w.

The macrostructure of the pad might be designed and fabricated so that the number of pores of a few micrometers in the pad are reduced and the larger-size pores, about 50 - 80 μm, distributed more uniformly. The elimination of the small pores prevents particles accumulating in the pores that might act like a larger size particle. This is likely to control the particle size by retaining a small distribution, larger number of small abrasives on the active

material removal mode to reduce the formation of large scratches. Features like larger pores, around 50 -80 μm, will help local slurry dispensing and collect agglomerates to keep the mean abrasive size small. If the larger pores can be produced with a better distribution, both in size and location, a better local slurry transfer and efficient replacement of the worn particles might help to increase k_w. By combining the porosity with the pad-scale features, like the x-y or concentric grooves about 250 μm wide and 380 μm deep on the existing pad which improves the wafer-scale slurry dispensing, the MRR, WIWNU, and surface roughness might be all improved at the same time.

3.5 Conclusions

Theories of polishing processes such as surface melting, plastic deformation, brittle fracture and burnishing were reviewed. Each theory was examined for friction coefficient, material removal rate, Preston constant, wear coefficient, and the topography of the worn surface. Wafers coated with Al, Cu, SiO_2 (PECVD and TEOS) and Si_3N_4 were tested under typical CMP conditions with Al_2O_3 neutral slurry. Based on the experimental results and the theoretical models the following conclusions are drawn.

(1) For all coatings tested, the friction coefficient remained at a low and constant level, around 0.1 - 0.3. It was close to the value predicted by the plastic deformation model.

(2) The prevailing mechanism of material removal in fine abrasive polishing is plastic deformation. Surface melting does not occur because the temperature rise is marginal. Brittle fracture was not observed because the normal load on the abrasive particle is below the critical value for fracture. Moreover, burnishing does not play a significant role in removing material since the work of adhesion is extremely low.

(3) The MRR, NMRR and Preston constant were inversely proportional to the hardness of the coatings. The wear coefficient was about 10^{-4} for the materials polished. The effect of pad stiffness was marginal compared with that of the coating hardness.

(4) The microcutting model yielded a higher value of MRR and wear coefficient ($\sim 10^{-2}$) than the experiments. The discrepancy was explained on the basis of the small penetration depth of the particle, due to the small abrasive employed, the lighter load on the abrasive, due to the wafer/pad direct contact, and particle rolling.

(5) A stiffer pad resulted in a better wafer-scale uniformity, or a lower WIWNU. For PECVD SiO_2, TEOS SiO_2 and Si_3N_4 coatings, the WIWNU remained at an acceptable low level, less than 2.5% after polishing.

(6) The size effect of the abrasive increased the MRR and wear coefficient. The MRR increased about 2.6 times with the increase of particle size from 50 nm to 1000 nm. The surface roughness however increased at a slower rate, about 1.6 times, and remained below an acceptable level, about 20 nm.

(7) The size and the density of scratches increased with abrasive size while the roughness for the abrasive sizes employed, 50 nm, 300 nm and 1000 nm, was maintained well below the lithography tolerance. It was observed that a few deeper scratches, about 20-50 nm, were scattered on all sample surfaces.

(8) The pressure-velocity product and the Preston constant must be optimized to enhance the MRR. The lower wear coefficient of experiments, about two orders of magnitude smaller than the theoretical estimation, throws light on improvements to the Preston constant. It is able to increase the wear coefficient through the mechanical, such as increasing the abrasive size or fixing abrasive particles, or the chemical-mechanical approaches, such as using moderate acidic solution on Cu, in the future.

(9) It is also important to retain the WIWNU, surface roughness and scratching at a acceptable low level. Optimization schemes such as increasing the pad stiffness, choosing pressure-velocity regime, and designing the macrostructure of the pad to improve slurry dispensing were proposed to reduce the WIWNU. On the other hand, the surface roughness and scratching may be reduced by using fine-grade abrasives, narrowing the abrasive size distribution, and re-designing the pad micro- and macro-structures to control agglomeration.

Nomenclature

A = apparent area of contact (m^2)
a = side length of a square contact (m)
b = radius of the plastic zone of abrasive indentation (m)
c = length of lateral crack (m)
d = depth of surface groove (m)
E = Young's modulus of coating material (N/m^2)
F = tangential force on the wafer (N)
f_n = normal force on the abrasive particle(N)
f_a^* = transition threshold of normal force on the abrasive particle (N)
H = hardness of coating material (N/m^2)
h = thickness of the material removed on wafer surface (m)
K_c = fracture toughness of coating material ($Pa\sqrt{m}$)
k_1, k_2 = thermal conductivity (W/m·K)
k_p = Preston constant (m^2/N)
k_w = wear coefficient
L = normal load on wafer (N)
l = sliding distance of the abrasive particle at one pass (m)
p = normal pressure on wafer (N/m^2)
∂ = peak load on the abrasive particle in an indentation cycle (N)
Q, Q_1, Q_2 = rate of frictional heat (W)
q = frictional heat flux (W/m^2)
R_a, R_q = mean value and root-mean-square of surface roughness (m)
r = radius of abrasive particle (m)
r^* = critical radius of abrasive particle (m)
S = sliding distance (m)
s = interfacial shear stress due to adhesion (N/m^2)
T_f, T_o = flash and bulk temperature of contact (K)
t = experiment duration (s)
V = volume loss (m^3)
v_R = relative linear velocity of wafer (m/s)
W_{ab} = work of adhesion of the contacting materials(N/m)
w = width of groove (m)
α_1, α_2 = material-dependent constants

$\gamma_a, \gamma_b, \gamma_{ab}$ = surface energy of solids (N/m)

κ = numerical constant

μ = friction coefficient

ν = Poisson's ratio

θ = angle between the abrasive and the surface (rad)

References

Aghan, R.L. and Samuels, L.E., 1970, "Mechanisms of Abrasive Polishing," *Wear*, Vol. 16, pp. 293-301.

Archard, A.J.G., 1958, "Contact and Rubbing of Flat Surfaces," *J. Applied Physics*, Vol. 24, pp. 981-988.

Beilby, Sir George, 1921, *Aggregation and Flow of Solids*, Macmillan & Co., London.

Bowden, F.P. and Hughes, T.P., 1937, "Physical Properties of Surfaces IV - Polishing, Surface Flow and the Formation of the Beilby Layer," *Proc. Roy. Soc*., Vol 160A, pp. 575-587.

Bowden, F.P. and Tabor, D., 1950, *The Friction and Lubrication of Solids*, Clarendon Press, Oxford, Part I, pp. 52 -57.

Brown, N.J., Baker, P.C., and Maney, R.T., 1981, "Optical Polishing of Metals," *Proc. SPIE*, Vol. 306, pp. 42-57.

Buijs, M., and Houten, K.K., 1993, "Three-Body Abrasion of Brittle Materials as Studied by Lapping," *Wear*, Vol. 166, pp. 237-245.

Bulsara, V.H., Ahn, Y., Chandrasekar, S., and Farris, T.N., 1998, "Mechanics of Polishing," ASME *J. Applied Mechanics*, Vol. 65, pp. 410-416.

Cook, L.M., 1990, "Chemical Process in Glass Polishing," *J. Non-Crystalline Solids*, Vol. 120, pp. 152-171.

Evans, A.G. and Marshall, D.B., 1980, "Wear Mechanisms in Ceramics," *Fundamentals of Friction and Wear of Materials, ASM*, pp. 439-452.

Goddard, J. and Wilman, H., 1962, "A Theory of Friction and Wear during the Abrasion of Metals," *Wear*, Vol. 5, pp. 114-135.

Hokkirigawa, K. and Kato, K., 1988, "An Experimental and Theoretical Investigation of Ploughing, Cutting and Wedge Formation during Abrasive Wear," *Tribol. Int*., Vol. 21, pp. 51-57.

Holm, R., 1946, *Electric Contacts*, Almqvist and Wiksells, Stockholm.

Jaeger, J.C., 1942, "Moving Sources of Heat and the Temperature at Sliding Contacts," *J. Proc. Royal Soc. N. South Wales*, Vol. 76, pp. 203-224.

Komanduri, R., Lucca, D.A., and Tani, Y., 1997, "Technological Advances in Fine Abrasive Process," *Annals CIRP*, Vol. 46, pp. 545-596.

Komvopoulos, K., Saka, N., Suh, N.P., 1985, "The Mechanism of Friction in Boundary Lubrication, " ASME *J. Tribology*, Vol. 107, pp. 452-461.

Lim, S.C. and Ashby, M.F., 1986, "Wear-Mechanism Maps," *Acta Metall*., Vol. 35, pp. 1-24.

Liu, C.-W., Dai B.-T., Tseng, W.-T., and Yeh, C.-F., 1996, ”Modeling of the Wear Mechanism during Chemical-Mechanical Polishing,” *J. Electrochem. Soc.*, Vol. 143, pp. 716-721.

Luo, Q., Ramarajan, S., and Babu, S.V., 1998, “Modification of Preston Equation for the Chemical-Mechanical Polishing of Copper,” *Thin Solid Films*, Vol. 335, pp. 160-167.

Mulhearn, T.O. and Samuels, L.E., 1962, “The Abrasion of Metals: A Model of the Process,” *Wear*, Vol. 5, pp. 478-498.

Newton, Sir Isaac, 1695, *Opticks*, Dover Publication, Inc., New York, 1952, based on the 4th ed., London published in 1730.

Preston, F.W., 1927, “The Theory and Design of Plate Glass Polishing Machines,” *J. Soc Glass Technology* , Vol. 11, pp. 214-256.

Rayleigh, Lord, 1901, “Polish,” *Nature*, Vol. 64, pp. 385-388.

Rabinowicz, E., 1968, “Polishing,” *Scientific American*, Vol. 218, pp. 91-99.

Runnel, S.R. and Eyman, L.M., 1994, “Tribology Analysis of Chemical-Mechanical Polishing,” *J. Electrochem. Soc.*, Vol. 141, pp. 1698-1701.

Samuels, L.E., 1971, *Metallographic Polishing by Mechanical Methods*, 2nd ed., Elsevier, New York.

Sin, H.-C., Saka, N., Suh, N.P., 1979, “Abrasive Wear Mechanisms and the Grit Size Effect, “ *Wear*, Vol. 55, pp. 163-190.

Suh, N.P., 1986, *Tribophysics*, Prentice-Hall, Inc., Englewood Cliffs, New Jersey, pp. 14-17.

Sundararajan, S., Thakurta, D.G., Schwendeman, D.W., Murarka, S.P. and Gill, W.N., 1999, “Two-Dimensional Wafer-Scale Chemical Mechanical Planarization Models Based on Lubrication Theory and Mass Transport,” *J. Electrochem. Soc.*, Vol. 146, pp. 761-766..

Yu, T.-K., Yu, C.C., and Orlowski, M., 1993, “A Statistical Polishing Pad Model for Chemical-Mechanical Polishing,” *Proc. 1993 IEEE Int. Electron Dev. Mfg.*, pp. 865-868.

Appendix 3A Flash Temperature at the Particle/Wafer Contact in Polishing

When two surfaces slide relatively, most of the work is converted into heat. The rate of this frictional heat generated per unit nominal contact area, q, can be expressed as:

$$q = \frac{\mu L v_R}{A} \tag{3A.1}$$

where μ is the friction coefficient of sliding, L the normal load, v_R the relative sliding velocity, and A the apparent area of contact. In reality, the heat is dissipated into the bulks via the contact area, usually a very small fraction of the apparent surface area. In abrasive polishing, it may be assumed that the friction heat diffuse only into the abrasive and the coating surfaces, and steady state can be reached at the contact. The boundary condition which assumes that the temperature far away from the contact remains at a constant bulk temperature (approximately room temperature) is convenient in polishing. The heat capacity of the pad and the wafer backing is large and the temperature rise is insignificant.

A portion of the frictional heat, Q_1, flows into the coating being polished, and Q_2 into the abrasive/pad. The total heat generation is (Bowden and Tabor, 1950):

$$Q = \mu f_n v_R = Q_1 + Q_2 \tag{3A.2}$$

Q_1 and Q_2 can be expressed as the product of thermal conductance of the contact and temperature rise. For circular contact with contact width w, the thermal conductance is $2wk$, thus Q_1 and Q_2 can be rewritten as:

$$Q_1 = 2wk_1(T_f - T_o), \text{ and} \tag{3A.3a}$$

$$Q_2 = 2wk_2(T_f - T_o). \tag{3A.3b}$$

Combining Eqs. (3A.2), (3A.3a) and (3A.3b), the flash temperature is given as:

$$T_f = T_o + \frac{\mu f_n v_R}{2w} \frac{1}{k_1 + k_2} \tag{3A.4}$$

This is close to the results given by Jaeger for a square junction of side *a* at low sliding speed in a more rigorous analysis (Jaeger, 1945):

$$T_f = T_o + \frac{\mu f_n v_R}{2.12a} \frac{1}{k_1 + k_2}. \tag{3A.5}$$

Appendix 3B Polishing due to Microcutting

The upper bound analyses for the friction coefficient and estimates for material removal rate in the microcutting mode idealized the shape of the abrasive tip as a cone or a sphere (Goddard and Wilman, 1962; Sin et al., 1979; Komvopoulos et al., 1984).

For a conical tip of abrasive particles, as shown in Fig. 3B.1(a), the depth and width of cut are related by:

$$d = \frac{w}{2}\tan\theta \tag{3B.1}$$

where d is the depth of the grooves, w the width of the grooves and θ the angle between the abrasive and the surface. The normal force, f_n, on the particle is support by the pressure, p, at the contacting interface, which is assumed to be the pressure on the soft surface at yielding. Since only the front half of the cone is in contact while sliding, the normal force can be calculated simply by multiplying the projected area of the contacting surface with the pressure at yielding of the worn surface. Thus:

$$f_n = \frac{\pi w^2}{8} p \tag{3B.2}$$

Similarly, the frictional force may be written as:

$$f_t = \frac{w^2}{4} p\left(\tan\theta + \frac{s}{p}\sec\theta\right) \tag{3B.3}$$

where s is the interfacial shear stress due to adhesion. Combining Eqs. (3B.2) and (3B.3), the friction coefficient can be written as:

$$\mu = \frac{2}{\pi}\left(\tan\theta + \frac{s}{p}\sec\theta\right) = \frac{2}{\pi}\left(\tan\theta + \frac{s}{H}\sec\theta\right) \tag{3B.4}$$

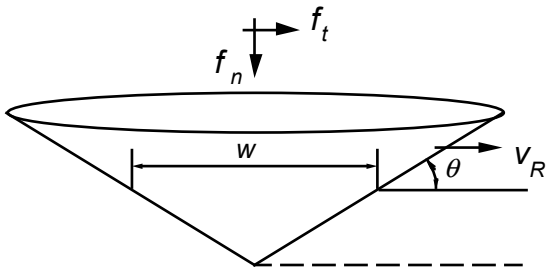

(a)

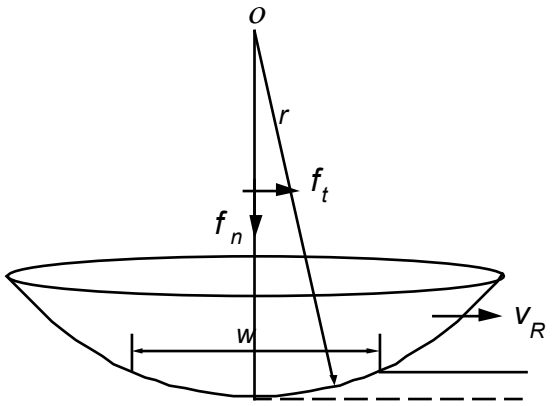

(b)

Figure 3B.1 Schematics of microcutting model in polishing: (a) with conical shape abrasive, (b) with spherical shape abrasive. (from Komvopoulos et al., 1984)

In the above equation the yield pressure is approximated as the hardness, H, of the worn surface. The material removed can be estimated by the product of the cross section of the groove, $dw/2$, and the sliding distance of the particle, S. The wear coefficient thus can be determined by Eq. (3B.3) as:

$$k_w = \frac{VH}{LS} = \frac{(dwS/2)H}{f_n S} = \frac{\tan\theta}{2\pi} \tag{3B.5}$$

The surface roughness due to microcutting is of the same order of magnitude as the depth of the groove:

$$R_a \approx \frac{d}{2} = \frac{w}{4}\tan\theta \tag{3B.6}$$

The same treatment can be applied to an abrasive with a spherical tip, as shown in Fig. 3B.1(b), which might be closer to the actual shape of the abrasive particles. The geometry of the groove can be related to the radius of the particles, r, by:

$$r^2 = (r-d)^2 + (w/2)^2 \tag{3B.7}$$

In polishing, the penetration is usually very shallow. Therefore Eq. (3B.7) can be simplified and the depth of the groove can be approximated by:

$$d = \frac{w^2}{8r} \tag{3B.8}$$

The normal and tangential forces acting on the particle to produce plastic flow can be determined as before. Thus:

$$f_n = \frac{\pi w^2}{8} H \tag{3B.9}$$

$$f_t = Hr^2\left\{\sin^{-1}\frac{w}{2r} - \frac{w}{2r}\left[1-\left(\frac{w}{2r}\right)^2\right]^{1/2}\right\} + 2sr^2\left\{1-\left[1-\left(\frac{w}{2r}\right)^2\right]^{1/2}\right\} \tag{3B.10}$$

$$\mu = \frac{2}{\pi}\left(\frac{2r}{w}\right)^2\left\{\sin^{-1}\frac{w}{2r} - \frac{w}{2r}\left[1-\left(\frac{w}{2r}\right)^2\right]^{1/2}\right\} + 2\frac{s}{H}\left\{1-\left[1-\left(\frac{w}{2r}\right)^2\right]^{1/2}\right\} \tag{3B.11}$$

$$k_w = \frac{2}{\pi}\left(\frac{2r}{w}\right)^2\left\{\sin^{-1}\left(\frac{w}{2r}\right) - \left(\frac{w}{2r}\right) + \frac{1}{2}\left(\frac{w}{2r}\right)^3\right\} \tag{3B.12}$$

The surface roughness may be expressed as:

$$R_a \approx \frac{d}{2} = \frac{f_n}{2\pi rH} \tag{3B.13}$$

Appendix 3C Polishing due to Brittle Fracture

In this mode of polishing, shown in Fig. 3C.1, the elastic/plastic stress field that governs crack development is influenced by hardness and elastic modulus in addition to the toughness of the contacting material. Brittle fracture due to lateral cracking occurs when the load on the particle reaches a transition threshold, f_n^*, which is characterized by (Evans and Marshall, 1980):

$$f_n^* = \kappa \left(\frac{K_c^4}{H^3} \right) f(E/H) \tag{3C.1}$$

where κ is a dimensionless constant, K_c the toughness, H the hardness, and E the Young's modulus of the material been polished. $f(E/H)$ is a function that depends on the type of crack. For lateral cracks, $f(E/H)$ varies slowly with E/H and $\kappa f(E/H)$ is approximately 2×10^{-5}. Once the crack initiates, it extends due to the peak load, $\hat{p}$, in the indentation cycle. For a plastic groove in a sliding particle contact, the lateral crack length, c, is given by:

$$c = \alpha_1 \left[\frac{(E/H)^{3/5}}{K_c^{1/2} H^{1/8}} \right] \hat{p}^{5/8} \tag{3C.2}$$

where α_1 is a material-independent constant. The lateral fracture depth typically scales with the plastic zone radius b, which relates to the plastic indentation width, w, by:

$$b \sim w(E/H)^{2/5} \tag{3C.3}$$

The indentation width depends on the peak normal pressure $\hat{p}$ on the particle and the hardness of the polished material:

$$w \sim (\hat{P}/H)^{1/2} \tag{3C.4}$$

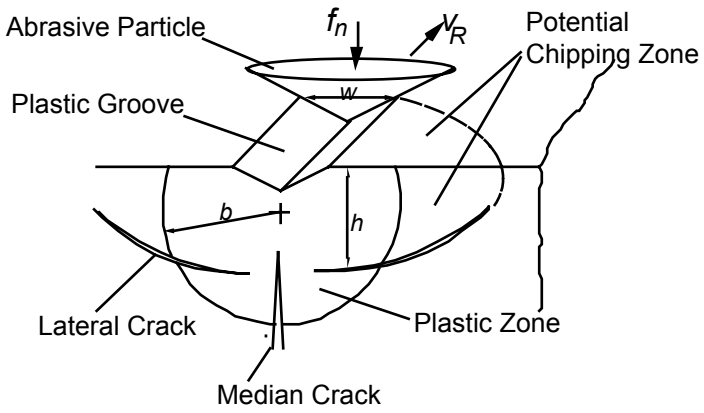

Figure 3C.1 Schematic of the mechanisms of brittle fracture in polishing with lateral cracks (after Evans and Marshall, 1980).

Assuming wear particles can be generated by single-cycle particle contact and that peak pressure is approximated to the average pressure on the abrasive particle, the wear volume per particle can be estimated by Eqs (3C.2) to (3C.4) and written as:

$$V = \alpha_2 l \frac{f_n^{9/8}}{K_c^{1/2} H^{5/8}} (E/H)^{4/5} \tag{3C.5}$$

where α_2 is another material-independent constant determined by experiments and l the sliding distance of the pass. The wear coefficient can thus be expressed as:

$$k_w = \alpha_2 \frac{f_n^{1/8} H^{3/8}}{K_c^{1/2}} (E/H)^{4/5} \tag{3C.6}$$

When the load on the particle is below the threshold in Eq. (3C.1), material is removed by a plastic cutting process.